PlagCheck: no concerns
Tables?: 4
Word Count: 7200
Prod Note: check blk/eq/supple callouts/

Revision 1 (8698)

A rare sekaninaite occurrence in the Nenana Coal Basin, Alaska Range, Alaska

Stephen P. Reidel

Pacific Northwest National Laboratory, Retired

Richland, WA 99352

Sreidel105@gmail.com

Martin E. Ross

Martin E. Ross, Professor emeritus, Department of Marine and Environmental Sciences, Northeastern University, Boston, Massachusetts 02115

Martyross43@gmail.com

Running title: Sekaninaite in the Alaska Range

Abstract

Coal-seam fires are not uncommon and occur in coal deposits of all ages. Coal-seam fires have been noted in Alaska, but this paper is the first to describe the mineralogy and petrology of a coal-seam fire in the Mystic Creek coal basin in the remote eastern part of the Nenana Coal Basin, Alaska Range. The coal is Miocene and part of the Healy Creek Formation of the Usibelli Group. The coal-fire products were studied optically and analyzed using XRF, XRD, and electron microprobe. The host rock is a silty sandstone consisting mainly of quartz, feldspar, and minor hematite and clay. The coal-seam fire fused and melted the country rock producing a metasediment-clinker and paralava. Sekaninaite, plagioclase, and fayalite are the main minerals that formed along with titanomagnetite, mullite, augite and an unidentified Al-Fe-Ti oxide mineral. Petrographic analysis shows there are at least three distinct lithologies in the paralava at thin section scale: a vesicular, holocrystalline sekaninaite-plagioclase $\pm$ olivine bearing area; holocrystalline areas dominated by plagioclase and quartz $\pm$ minor sekaninaite; glassy bodies; and a bulbous, lenticular body of course sekaninaite and lesser olivine. The paralava is an andesite with rhyolitic residual glass. Oxidation and fusion of the sediment was the first phase of pyrometamorphism where the sediment becomes brown-red and sekaninaite begins to form. The metasediment melts forming vesicles in a black glass; sekaninaite formation is well underway. The melt separates from the host and coalesces to form the paralava. As the paralava cools, fayalite and sekaninaite precipitate accompanied by plagioclase, quartz, titanomagnetite and an Al-Fe-Ti oxide. Proximity to the surface allowed quenching of the remaining liquid to rhyolitic glass. Numerical modeling was employed to calculate the liquidus temperature (1140^{o} to 1200^{o}C) and understand the crystallization pathway to the rhyolitic glass. In all models, sekaninaite precipitation is the most important mineral leading to the rhyolitic glass.

Keywords: Sekaninaite, Nenana Coal Basin, Alaska Range

Introduction

Coal-seam fires have occurred world-wide throughout geologic time (e.g. Sen, 1957; Wahrhaftig et al., 1969; Foit et al., 1987; Cosca et al., 1989; Sharygin et al., 1999, 2009, 2014; Grapes, 2011; Grapes et al. 2009, 2011; Thiéry et al., 2018,; Guy et al. 2020). There is abundant evidence for fires that have since burned out and others that have burned for decades and even thousands of years (Sharygin et al., 2014). In this study we investigate a prehistoric coal-seam fire in the Nenana coal basin in the Alaska Range (Fig. 1). Although coal-seams in the western part of the basin near the Alaska Railroad and Richardson Highway have been mined and studied, the eastern part is remote and relatively inaccessible except by helicopter. The Mystic Creek coal basin in the remote eastern part, is the subject of our study.

Geologic Setting and Background

The coal-bearing rocks of the Nenana Coal Basin occur in a series of faulted synclines in an extensional basin in the northern foothills of the central Alaska Range (Fig. 1) (e.g. Wahrhafrig, 1970a, b, c, d, e, f, g, h). The basin lies north of the Farewell-Denali Fault and within the Tintina Gold Province. The stratigraphy consists of pre-Cenozoic metamorphic rocks overlain by Eocene to Pleistocene sedimentary rocks that were folded and faulted as the Alaska Range began growing in the Miocene. The Usibelli Group comprise Cenozoic sediments that make up the coal field; they rest on an eroded complex of Paleozoic to Cretaceous greenschist grade metavolcanic and metasedimentary rocks (Wahrhaftig et al. 1969; Kirschner, 1994; Ducel-Bacon et al., 2007; Wartes et al. 2013). Cretaceous plutonic and Precambrian rocks lie farther south in the heart of the Alaska Range. Pliocene and Pleistocene gravels and alluvium overlie parts of the coal field.

The Usbelli Group (Fig. 2) consists of five formations: the Healy Creek, Sanctuary, Suntrana, Lignite Creek and Grubstake Formations. Prior to uplift of the Alaska Range, sediments were deposited by a southward flowing drainage system (Wahrhaftig et al. 1969). The growth of the Alaska Range diverted the drainage system westward, much like it is today.

The Healy Creek Formation is probably the most widely distributed formation of the lower coal-bearing formations of Wahrhaftig et al., (1951). It lies unconformably on mainly Paleozoic metamorphic rocks of the Yukon-Tanana terrane (Wahrhaftig, 1987; Wilson and others, 1998) and consists of interbedded poorly consolidated sandstone, conglomerate, claystone and coal beds. Although these rock units are mainly Miocene in age, Leopold and Lui (1994) suggest the lower part may be late Oligocene. Wolfe and Tania (1987) suggest that the sediment of the Rex Creek area may be as old as Eocene.

The Sanctuary Formation lies conformably on the Healy Creek Formation (Fig. 2) and consists of gray shale that weathers to a chocolate brown or yellow brown; the upper part is silty with fine sand beds that probably accumulated in a shallow lake (Wahrhaftig et al. 1969). Coal beds are abundant throughout the unit.

The Suntrana Formation conformably overlies the Sanctuary Formation and is estimated to contain the bulk of the coal reserves (Wahrhaftig et al. (1969). It consists of a series of repeated coarse pebbly sandstones grading upward into fine sands and claystone and coal, suggesting that it formed in a basin that alternated between a coal-forming basin and periods when a braided fluvial system flowed from the north (Wahrhaftig et al. 1969). Based on paleobotany, Wolfe and Tanai (1980) dated the Suntran~~t~~a Formation as Middle Miocene Seldovian floristic stage (Fig. 2). Triplehorn et al. (1999) obtained an$_{40}$Ar/$_{39}$Ar date of 32 Ma on a kaolinitic clay layer in coal layer #6 near the top of the uppermost unit. However, based on inconsistency of the data and low radiogenic content of most samples, they considered the date to be unreliable.

The Lignite Creek Formation conformably overlies the Suntrana Formation and includes interbedded sandstone, claystone, and thin coal beds. It comprises two facies: a coal-bearing facies in the southern basin and a noncoal-bearing facies in the northern basin. The coal beds are mostly thin and discontinuous.

The Grubstake Formation rests conformably on the Lignite Creek Formation and is overlain by the Nenana gravels of Pliocene to early Pleistocene (Sortor et al., 2021). The Grubstake Formation consists of interbedded claystones, sandstones, and fine conglomerates. Coal occurs locally and is typically thin bedded. Two thick ash beds occur in the formation (Fig. 2). Wahrhaftig et al. (1969) obtained an 8.1 Ma K/Ar radiometric date on glass from the lower ash. Triplehorn et al. (1999) reanalyzed the ash using $_{40}$Ar/$_{39}$Ar dating techniquesand got an age of 8.3 Ma, but they considered this to be in error due to excess Ar in the glass. Minerals from the glass were also age-dated by Triplehorn et al. (1999) which gave apreferred age of 6.7 Ma.

Coal of the Nenana Basin

The coal of the Healy Creek area has been classified as subbituminous B and C (Cooper et al. 1946). Coal in the Lignite Creek Formation is classified as subbituminous C and lignite (Martin, 1919). These classifications were made for the active coal mining areas in the accessible western part of the basin. The coal is typically black to dark brown with a dull luster. Fossil twigs are found locally at the tops of many layers. Coal near the base of the base Healy Creek Formation is higher in heating values than that near the top (Wahrhaftig et al. 1969). Most of the coal has an ash content estimated to be between 10% and 20%.

Wahrhaftig et al. (1969) reported that during his field work (1940s), there were several active coal-seam fires. The most prominent prehistoric and widespread burnt coal seam within the Nenana coal basin is in the C&D layers of the Healy Creek Formation (Fig.3). Warters et al. (2013, Fig. 3) also identified a burned coal in the Suntrana Formation. A large but indeterminable amount of coal had been lost there due to coal-seam fires. Burning coal has baked overlying sediments, especially the clay and shale layers.

Coal-seam fires in the Nenana basin are not unusual today. One fire in 2009 was responsible for the Rex Creek wildfire; four coal-seam fires were reported in 2016 (Hollander, 2016); two coal-seam fires in the Healy Creek area merged in 2018 to form the Healy Creek wildfire that covered over 1,800 acres (Ellis, 2018). No coal-seam fires have been reported from the remote eastern part of the basin but field work as part of this study showed evidence of past fires.

Methods

We sampled a burnt coal seam in the largely inaccessible Mystic Creek coal basin that is over 50 km east of Healy. The basin lies in a synclinal trough near the Wood River (Fig. 1) and is a small eroded remanent in the Nenana basin. The sampling sites are about 2 m above the Mystic Creek stream bed. Wahrhaftig et al. (1969) states that the Healy Creek Formation forms the base of Mystic Creek where itis approximately 330 m thick. Based on Wahrhaftig's (1969) description, we interpret our sampling site to be in the Healy Creek Formation and possibly equivalent to coal beds C&D (Fig. 3) although we cannot show a direct correlation because the basin is isolated and the stratigraphy there has not been refined.

Based on our samples (Fig. 4), the authors originally thought the locality was a lava flow that invaded wet sediment and baked the sediment into a clinker, like invasive Columbia River Basalt Group (CRBG) flows (e.g. Ross, 1989; Reidel et al. 2013). Invasive CRBG flows are common where the basalts are erupted onto thick, unconsolidated sediments. The flows burrow into the sediments and can bake the sediment in contact resembling our sample sites. We now recognize that these sites resulted from a coal-seam fire. The sample in Figure 4 resembles paralavas and clinker in Figures. 2 and 3 of Guy et al. (2020). A paralava is a pyrometamorphic rock that is vesicular, aphanitic, often pahoehoe like and with clear flow structures. We define the clinker as a mixture of the stony residual and baked sediment that is slightly metamorphosed. We analyzed both the paralava (RR21-1) and the intercalated metasediment-clinker (RR1SED-1).

Petrography

Paralava

Overall, the paralava is a very fine-grained to glassy rock. Petrographic analysis shows there are at least three distinct lithologies (Fig. 5) present in the Mystic Creek coal basin paralava on a thin section scale : a vesicular, holocrystalline sekaninaite-plagioclase $\pm$ olivine bearing area (SP domains), holocrystalline areas (PQ domains) dominated by plagioclase and quartz $\pm$ minor sekaninaite, and lenticular shaped glassy bodies (G domains). A bulbous, lenticular body of coarse sekaninaite + lesser olivine (CS on Fig. 5) may represent a fourth domain or may be just a minor phase of the SP domain.

Vesicular SP domains consist of sekaninaite, plagioclase, titanomagnetite, an Al-Fe-Ti oxide mineral that we are unable to identify, and lesser olivine and make up the dominant lithology forming the matrix surrounding the glassy, lenticular G domains, and the SQ domains. The sekaninaite (Figs. 6a, 6b. and 6d) occurs as subhedral to anhedral, equant to elongate grains with good cleavage (100) and 001 parting. It is biaxial negative with 2V~60^o to 65^o, inclined extinction, 90^o prismatic cleavage, moderate birefringence, and is pale greenish with reddish-brown alteration (hematite?) on cleavages. A bulbous, lenticular body (CS on Fig. 5) of coarse sekaninaite occurs within a much finer-grained, vesicular body of plagioclase, opaque oxides, and sekaninaite (Fig. 6g). The sekaninaite in the lenticular body has hematite on cleavages and occurs with abundant tiny opaque oxide grains.

Olivine (Fig. 6a) has a higher birefringence than the sekaninaite and is biaxial negative with a 2V>70^o. It is anhedral with slightly curved partings resembling cleavage. It is typically pale green to pale yellow-brown with brown alteration (hematite?) on partings.

The PQ domains form as patches and border zones along the margins of the glassy bodies and as veins and lobes invading them (Figs. 6c, 6d and 6h). The PQ domains consist of plagioclase (59.4%), quartz (9.7%), titanomagnetite and the unidentified Al-Fe-Ti oxide mineral (together =

30.9%), and possibly sekaninaite as grains too small for positive identification (Table 1). The plagioclase forms tiny slender lath-shaped microlites and less commonly occurs as clusters of larger grains up to 0.4mm in diameter along the margins of the glassy bodies (Fig. 6e). Scattered alkali feldspar grains have slightly higher birefringence (1^{st} order yellow) than the plagioclase, are biaxial negative and have an estimated 2Vgreater than 60^{o}. Opaque grains are abundant as small, square euhedral grains. The PQ domains generally coarsen along the margins of the glassy bodies. They appear to be derived from a sekaninaite-bearing lithology by reaction with glassy bodies. Evidence for this transition occurs where a vein extending from the SP domain abruptly becomes a PQ domain where it enters a glassy body (Fig. 6c). Two larger augite grains within the felsic areas are present (Fig.6f).

The three irregular to lenticular glassy bodies forming the G domains (Fig. 5) consist of yellow-brown vesicular rhyolitic glass containing lath-shaped plagioclase (15.1%), sharp, angular fragments of quartz (10.3%), opaque oxides (2.0%), and a trace of brownish sekaninaite. The bodies are invaded by veins and lobes of the PQ domain which also borders them (Figs. 6c and 6d). The lenticular shapes of the glassy bodies (Fig. 5) and their invasion by the PQ domain suggests both were mobile which is supported by the physical flow structure of the sample (Fig. 5). The glassy bodies resemble magma pillows formed when mafic magma invades a granitic magma or crystal mush and are separated into rounded to lenticular segments and invaded by veins and lobes of the granitic liquid (Ross, 2009, 2014).

Clinker-Metasediment

The clinker consists of reddish-brown areas intimately intertonguing with black areas (Figs. 7 and 8c). We interpret the red-brown areas as oxidized parts of the original sediment that has undergone slight metamorphism. The black areas are the initial melting of the clinker and typically are vesicular, containing abundant anhedral quartz grains, a feldspar (biaxial negative, 2V>60), titanomagnetite and possibly rare, tiny grains of sekaninaite set in a black, glassy matrix (Fig. 8a). Elongate vesicles and strings of small vesicles produce a flow or flattening fabric (Fig. 8b). The black areas closely resemble the glassy domains in the paralava. The red oxidized areas lack vesicles and contain less quartz than the black areas. The matrix consists of tiny, elongate original sediment fragments producing a distinct layering or bedding that is absent in the black areas.

Mineral chemistry

The mineralogy of the paralava sample was examined optically, by electron microprobe analyses, and Xray diffraction (XRD). Photomicrographs of many of the stations probed for chemical composition are shown in Figure 9. The dominant minerals present in the paralava are sekaninaite, olivine, feldspar, magnetite, an unidentified Al-Fe-Ti opaque oxide and quartz accompanied by glass. The mineral identifications were verified by XRD (Fig. 10) and microprobe analysis (Online Material Table OM1).

Plagioclase is the dominant mineral in the paralava from the Mystic Creek basin coal fire. Optically, it comprises 15 to 56.7 volume percent of the paralava (Table 1) and occurs as lath-shaped to irregular microlites. Albite twinning is rarely visible. Microprobe analyses indicate a consistent anorthite content of An96 to 98 and an absence of minor elements Ba, Ni and Mn. There is no noticeable zoning. X-ray diffraction patterns show a low intensity.

Sekaninaite is a rare mineral but is diagnostic in very high temperature pyrometamorphic rocks and is typically associated with tridymite, olivine, orthopyroxene, mullite, Fe-Ti oxides and occasionally cristobalite, feldspar, clinopyroxene and corundum. (Grapes et al., 2011; Sharygin, et al., 2014). In the Mystic Creek coal basin, sekaninaite accounts for 13.4 volume % of the SP domain (Table 1) and has SiO_2, FeO and Al_2O_3 compositions like those described by Grapes et al. (2011) and Sharygin et al. (2009) but higher MgO compositions. Analyses show Si lies within the low normal range (4.79-4.97 atoms per formula unit [apfu]) but with excess of Al (4.03-4.15 apfu). The MgO content of both Grapes et al. (2011) clinkers and the Mystic Creek coal basin metasediment/clinker are similar (~1-1.5 wt.%).

Olivine comprises approximately 12.3 volume percent of the SP domain in the Mystic Creek basin paralava. Analyzed olivines are iron-rich fayalites with contents consistently Fa90 (Online Material Table OM1).

Opaque minerals account for 17.6 to 30.9 volume percent of the Mystic Creek basin paralava (Table 1). We recognize titanomagnetite and an unidentified Al-Fe-Ti opaque oxide variety (Online Material Table OM1). The titanomagnetite typically contains as much as 50-57 wt.% TiO_2 and less than 8 wt.% Al_2O_3. The Al-Fe-Ti opaque oxide typically contains greater than 13 wt.% Al_2O_3 and less than 8 wt.% TiO_2. Microprobe analyses (Fig. 9; Online Material Table

OM1) have recognized numerous small grains but we have not established the mineral name. An X-ray diffraction pattern for the mineral is not apparent nor are the optic properties unique.

All glass analyses fall into the rhyolite field on the alkali-silica diagram of Lebas et al. (1986) (Online Material Table OM1; Fig. 11).

Whole Rock Chemistry

Both the paralava and enclosing metasediment host rock were analyzed for whole-rock compositions (Table 2). The country rock is a poorly consolidated silty sandstone with interbedded coal. The paralava and brown-red portion of the metasedimenthost rock were carefully sampled (Fig. 4) to ensure that chips of the paralava and host metasediment were analyzed separately. The bulk compositions of paralava and metasediment are similar and plot within the andesite field (Fig. 11). Both samples are moderate in SiO_2 high in Al_2O_3, K_2O, and low in Na_2O, CaO and MgO (Table 2).

Paragenesis

Analyses of the metasediment-clinker and paralava show the sequence of mineral formation as the country rock heated, began to melt and then crystallization as the paralava melt cooled.

The first phase of the pyrometamorphism is oxidation of the sediment (Figs. 4 and 7). The host sediment is poorly consolidated and white to beige but the sediment becomes brown-red (Fig. 7) from oxidation and begins to fuse. Thin sections and hand specimens show remnants of bedding and original quartz and feldspar. X-ray diffraction patterns (Fig. 10) show that sekaninaite is present suggesting that the temperature of formation of the metasediment was sufficiently high prior to fusion to form sekaninaite.

In the next phase, the brown-red metasediment begins to melt (black of Fig. 7) forming vesicles in a black glass. Vesicles probably formed as water in the sediment vaporized. Sekaninaite formation is well underway, but the dominant mineralogy is the original quartz, feldspar and titanomagnetite. Figures 7 and 8d show that the melt begins to separate from the host and coalesce to form veins of the paralava. The original bedding is destroyed by melting and the melt begins to flow like a normal lava (Fig. 4).

As the paralava begins to cool, which appears to be soon after formation, fayalite is the first mineral to precipitate accompanied by sekaninaite. Sekaninaite appears to continue to crystallize as the paralava cools. Plagioclase followed along with titanomagnetite, the Al-Fe-Ti oxide and quartz, The proximity to the surface allowed rapid cooling of the remaining liquid to form glass containing many microlites. However, we saw no evidence of roof collapse or opening of large cracks to the surface which is common for underground coal fires (Sharygn et al. 2014) resulting in rapid quenching of the paralava. This suggests that cooling and solidification proceeded at shower rate.

In the melt, the early forming holocrystalline minerals (SP domain) enclose the residual glassy domain (G domain) but initially remain mobile enough to invade the glassy area (Fig. 6c). Sekaninaite abruptly ceases forming where the holocrystalline vein enters the glassy domain. Veins from the plagioclase-quartz bearing domains (PQ domain) that formed as zones within the holocrystalline domain also invade the glassy zone (Fig. 6d). The plagioclase-quartz (PQ) domain minerals appear to begin crystallizing after the initial crystallization of the holocrystalline minerals. This suggests that water vapor may have allowed the earlier crystallization of the minerals in the holocrystalline domain. Upon elimination of water vapor, minerals within the plagioclase-quartz domain began forming.

Discussion

Coal-seam fires are not uncommon, occurring in coal deposits of any age. Coal-seam fires have been noted in Alaska, but this paper is the first to describe the mineralogy and petrology of a coal-seam fire in the Nenana coal basin.

The mineralogy of the Mystic Creek coal-seam fire is dominated by plagioclase and sekaninaite with lesser fayalitic olivine and two opaque minerals, titanomagnetite and an unidentified opaque Al-Fe-Ti oxide.

Temperature and Pressure

The Mystic Creek coal seam occurs approximately 300 m below the surface at ~1 atm pressure. The liquidus temperature can be estimated two ways. First, the occurrence of fayalite suggests that the temperature could be as high as 1200°C (Deer, Howie and zussman,1963, p.14) but undoubtly this is the lowest temperature reached in the coal fire. In the $FeO-SiO_2$ system of Bowen and Schairer (1932) and Schairer and Yagi (1952) (Fig. 12)as interpreted by Grapes et al. (2011), sekaninaite can first appear at 1210°C suggesting that the liquidus is approximately 1200°C. Fayalite forms a eutectic with tridymite and sekaninaite at 1083°C (Fig. 12). The fayalite-tridymite-albite eutectic is much lower at 980°C and approximates the composition of fayalite rhyolites.

A second method is to calculate the liquidus using MELTs with a QFM buffer (Ghiorso, and Sack,1995). Using this method, an equilibrium liquidus occurs at 1141°C. Considering both methods we estimate the liquidus temperature to lie between 1140- and 1200°C but much closer to 1200°C indicated by the presence of fayalite. These estimates are similar to that suggested by Sharygin et al. (2014) for the Ravat coal fire in Tajikistan where sekaninaite and fayalite also occur. This range represents the minimum high temperature reached by the Mystic Creek coal fire.

Bulk Paralava Composition.

The major, minor and trace element compositions of the paralava and the metasediment country rock are identical (Table 3) and plot in the andesite field (Fig.11) indicating that the paralava resulted from complete melting of the host sediment. All six microprobe analyses of the glass plot in the rhyolite field (Fig. 11). To compare the trace elements of the paralava and host sediment to estimates of the 'Bulk Earth,' we plott both on bulk Earth diagrams of Rudnick and Fountain (1995) and Hickley et al. (1986) (Fig.13). This also suggests that complete melting of the host sediment formed the paralava as both fit within the normal Bulk Earth except to lower Sr.

Modelling.

The coal-seam fire is effectively a closed system with complete melting of the host sediment. This provides a natural laboratory to model the evolution of the melt compositional from its initial composition to its residual glass under atmospheric conditions. The initial sediment and paralava compositions are identical and provide the starting composition, and the paralava glass composition provides the final liquid composition. We do not observe any residual sediment in the paralava supporting the conclusion that the melting of the sediment was complete. Our approach included several models: MELTs (Ghiorso and Sack, 1995), Magma Chamber Simulation (MCS, Boreson et al., 2020), and the least squares linear regression programs in Igpet (Carr and Gazel, 2017).

Magma Chamber Simulator (Boreson et al., 2020) was used to examine the possible fractionation path from parent (bulk host rock) to glass composition at1 atm. We calculated the equilibrium liquidus temperature (above) using MELTs and for use in MCS. After many runs, we could not successfully produce the rhyolite glass composition. In every case the final glass composition in MCS was a dacite. We concluded that MCS was not the appropriate model because we were trying to reproduce conditions at 1 atm when MCS was designed for much higher pressures. In addition, an important mineral, sekaninaite (Fe-Cordierite) was not one of the possible minerals in MCS.

The least squares linear regression model of Igpet (Carr and Gazel, 2017) was used in both the fractional crystallization mode and magma mixing mode (Tables 4 and 5). In the fractional crystallization mode, mineral compositions determined by electron microprobe analysis were fractionated from the parent composition (host rock – paralava) to produce the rhyolite daughter composition. In the magma mixing mode, the mineral compositions with the rhyolite glass compositions were 'mixed' to reproduce the bulk host metasediment-paralava composition (Table 3). To assess the residuals (differences between observed and calculated) we use one standard deviation of the rhyolite glass compositions. We chose this because the analyses for each mineral composition are similar but there are some differences in the microprobe analyses of the glass compositions. We concluded that this would be a better way to evaluate a model. The F value for the magma mixing equations is typically less than 1 and for the fractional crystallization mode, it is approximately 1. In the tables the residuals are typically less than the one standard deviation for the rhyolite glass.

The results of the least square-linear regression models were consistent in that sekaninaite is a dominant phase in both magma mixing and fractional crystallization modes. This may also explain why the MCS models were unsuccessful. In the fractional crystallization model (Table 4), sekaninaite is the main phase fractionated. In the mixing mode modes (Table 3), sekaninaite is mixed with the rhyolite glass in nearly equal proportions to represent nearly 95% of the equation. Although plagioclase is the dominant mineral determined optically, the glass contains microlites that are too small to recognize optically. The modeling suggests that the small microlites in the glass are mainly sekaninaite with some plagioclase, fayalite and the opaques as minor constituents. This appears to be supported by the X-ray diffraction patterns where sekaninaite forms prominent peaks compared to fayalite and plagioclase.

Implications:

Coal-seam fires represent an unusual and relatively unexplored natural environment of mineral formation in pyrometamorphic rocks. Although they are not uncommon, especially in the western USA, ones like the Mystic Creek coals that burned with an extremely high temperature (>1200^{o}C) and produce sekaninaite with fayalite are relatively rare. In addition, they provide a natural laboratory for understanding low pressure, high temperature fractional crystallization paths in magmas. Pyrometamorphic rocks often contain new minerals (e.g. Foit et al., 1987; Online Material Table OM1). It is not surprising that new mineral compositions previously unreported in nature have been discovered. Thus, pyrometamorphic rocks like the Mystic Creek coal basin provide a valuable natural laboratory for exploring magmatic processes and new minerals for future mineralogical studies.

Acknowledgments

We thank Leslie Baker, Warren Huff and an anonymous individual for reviewing this paper and providing valuable comments and suggestions. XRF analyses were provided by Dr. R Conrey, Hamilton College analytical labs; Electron Microprobe analyses were provided by Dr J Eckler, Yale University; XRD analysis was provided by Dr. Elitsa Hrischeva, Activation Laboratories Ltd.

References

Albanese, M.D. (1980) The geology of three extrusive bodies in the central Alaska Range: University of Alaska Fairbanks, unpublished Masters of Science thesis, 104 p.

Bohrson W.A., Spera, F.J., Heinonen. J.S.,Brown, G.A., Scruggs, M.A.,Adams J., Takach, M., Zeff, G., Suikkanen, E. (2020)Diagnosing open-system magmatic processes using the

Magma Chamber Simulator (MCS): part I—major elements and phase equilibria. Contributionsto Mineralogyand Petrology.175,29.https //doi.org/10.1007/s0041 0-020-01722

Carr, M.J., and Gazel, E. (2017) Igpet software for modeling igneous processes: examples of application using the open educational version. Contributions to Mineralogyand Petrology.111, 283–289. DOI 10.1007/s00710-016-0473-z

Cooper, H.M. Snyder, N.H., Abernethy, R.F., Tarpley, E.C., and Swingle,R.J. (1946)Analyses of mine, tipple, and delivered samples, in Analysis of Alaska coals. U. S. Bureau of Mines Technical Paper 682, p.20-22.

Cosca, M., Essene, E.J., Geissman, J.W., Simmons, W.B., Coates, D.A. (1989) Pyrometamorphic rocks associated with naturally burned coalbeds, Powder River Basin. Wyoming. American Mineralogist. 74, p.85–100

Deer, W.A., Howie, R.A., and Zussman, J. (1962) Rock Forming Minerals – Ortho- and Ring-Silicates.1st. ed. vol. 1. 333p. Longmans, Green and Co. LTD, London.

Dusel-Bacon, C., Aleinikoff, J.N., Premo, W.R., Paradis, S. and Lohr-Schmidt, I. (2007) Tectonic Setting and Metallogenesis of Volcanogenic Massive Sulfide Deposits in the Bonnifield Mining District, Northern Alaska Range.In Larry P. Gough and Warren C. Day, Eds. Recent U.S. Geological Survey Studies in the Tintina Gold Province, Alaska, United States, and Yukon, Canada—Results of a 5-Year Project, p.B1-B7. U.S. Geological Survey Scientific Investigations Report 2007–5289.

Ellis, T. (2018) Two coal-seam fires merge to form rapidly growing wildfire near Healy. Alaska National Public Radio, Station KUAC. https://www.alaskapublic.org/2018/06/20/two-coal-seam-fires-merge-to-form-rapidly-growing-wildfire-near-healy/#:~:text=Organization-,Two%20coal%2Dseam%20fires%20merge%20to,rapidly%2Dgrowing%20wildfire%20near%20Healy&text=State%20Forestry%20firefighters%20are%20working,the%20surface%20that%20merged%20together.

Foit, F.F., Hooper, R.L., and Rosenberg, P.E., (1987) An unusual pyroxene, melilite, and iron oxide mineral assemblage in a coal-fire buchite from Buffalo, Wyoming.American Mineralogist. 72, 137-147

Ghiorso, M. S., and Sack, R. O. (1995) Chemical Mass Transfer in Magmatic Processes. IV. A Revised and Internally Consistent Thermodynamic Model for the Interpolation and Extrapolation of Liquid-Solid Equilibria in Magmatic Systems at Elevated Temperatures and Pressures. Contributions to Mineralogy and Petrology. 119, 197-212.

Grapes R, Zhang K, Peng Z.L. (2009) Paralava and clinker products ofcoal combustion, Yellow River, Shanxi Province, China. Lithos. 113,831–843.

Grapes R, Korzhova S, Sokol E, Seryotkin Y. (2011) Paragenesis ofunusual Fe-cordierite (sekaninaite)-bearing paralava and clinkerfrom the Kuznetsk coal basin. Siberia, Russia Contributions to Mineralogy and Petrology. 162, 253–273.

Grapes, R. (2011) Anthropogenic Pyrometamorphism, in: Pyrometamorphism. Springer, 235-288.

Guy, B., Thiery, V.l Garcia, D., Bascou, J, and Broekmans, M. (2020) Columnar structures in pyrometamorphic rocks associated with coal-bearing spoil-heaps burned by self-ignition, La Ricamarie, Loire, France. Mineralogy and Petrology. 114,465–487.

Hickey, R.L., Frey, F.A. and Gerlach, D.C. (1986) Multiple sources for basaltic arc rocks from the southern volcanic zone of the Andes (34-41 S): Trace element and isotopic evidence for contributions from subducted oceanic crust, mantle and continental crust. Journal of. Geophysical. Research. 91, 5963-5983.

Hollander, Zag (2016) Four coal seam fires burning near Healy. Anchorage Daily Newshttps://www.adn.com/alaska-news/article/four-coal-seam-fires-burning-near-healy-include-new-start-old-burn-scar/2016/05/05/

Kirschner, C.E. (1994) Interior basins of Alaska. In Plafker, G., and Berg, H.C. Eds. The Geology of Alaska.The Geology of North America v. G-1, 469–493. Geological Society of America, Boulder, Colorado.

LeBas, M.J., LeMaitre, R.W., Streckeisen, A., and Zanettin, B. (1986) A chemical classification of volcanic rocks based on the total alkali silica diagram. Journal of Petrology. 27, 745-750.

Leopold, E.B. and Liu, G.(1994) A long pollen sequence of Neogene age, Alaska Range. In Ager,T.A., White, J.M., and Matthews, J.V. Jr. Eds.Tertiary Quaternary boundaries: 22–23, p.103–140. Quaternary International.

Martin, G.C. (1919) The Nenana coal field, Alaska. US. Geol. Survey Bulletin 664, 54 p.

Reidel, S.P., Camp, V.E., Tolan, T.L., and Martin, B.S. (2013) The Columbia River flood basalt province: Stratigraphy, areal extent, volume, and physical volcanology.In Reidel, S.P., Camp, V.E., Ross, M.E., Wolff, J.A., Martin, B.S., Tolan, T.L, and Wells, R.E., Eds., The Columbia River Flood Basalt Province,p. 1–43. Geological Society of America Special Paper 497. doi:10.1130/2013.2497(01).

Ross, M.E. (1989) Stratigraphic relationships of subaerial, invasive, and intracanyon flows of the Saddle Mountains Basalt in the Troy basin, Oregon and Washington.In Reidel, S.P. and Hooper, P.R. Eds.,Volcanism and Tectonism in the Columbia River Flood Basalt

Province, Geological Society of America Special Paper 497, p. 131–142. Boulder Colorado.

Ross, M. E. (1990) Mafic dikes of the Avalon Boston terrane, Massachusetts.IN Soccie, A.D., Skehan, and J. W., Smith, G. W., Eds., Geology of the composite Avalon terrane of New England, Geological Society of America, Special Paper 245, p. 133-153. Boulder Colorado.

Ross, M. E. (2014) Dike swarms of Cape Ann, Massachusetts. In Thompson, M.D., Ed., Guidebook to field trips in southeastern New England. MA-NH-RI. New England Intercollegiate Geological Conference. B4-1 to B4-22.

Rudnick, R.L. and Fountain, D.M. (1995) Nature and composition of the continental crust: A lower crustal perspective. Reviews in Geophysics, 33, 267–309. doi:10.1029/95RG01302

Schairer, J.F., Yagi, K.(1952) The system FeO-Al_2O_3-SiO_2. American Journal of Science, Bowen Vol 250A, 471–512.

Sen Gupta, S.(1957)Petrology of para-lavas of the eastern part ofJharia coalfield.The Quarterly journal of the Geological, Mining, and Metallurgical Society of India, 29, 79-101.

Sharygin, V.V., Sokol, E.V., Nigmatulina, E.N., Lepezin, G.G., Kalugin, V.M.,Frenkel, A.E. (1999) Mineralogy and petrology of technogenic parabasalts from the Chelyabinsk brown-coal basin. Russian Geology and Geophysics, 40, 879–899.

Sharygin, V.V., Sokol, E.V., Belakovski, D.I.(2009) Fayalite-sekaninaiteparalava from the Ravat coal fire (central Tajikistan). RussianGeology and Geophysics, 50, 703–721.

Sharygin, V. V., Sokol, E. V., Belakovsky, D.I. (2014) Mineralogy and Origin of Fayalite-Sekaninaite Paralava: Ravat Coal Fire, Central Tajikistan, in: Coal and Peat Fires: A Global Perspective, 582-607. doi:10.1016/B978-0-444-59509-6.00022-3

Sortor, R.N., Goehring, B.M., Bemis,S.P., Ruleman, C.A., Caffee, M.W., Ward, D.J. (2021) Early Pleistocene climate-induced erosion of the Alaska Range formed the Nenana Gravel. Geology, 49, 1473–1477. https:// doi.org/10.1130/G49094.1

Thiéry, V., Guy, B., Kruszewski, Ł., Carpentier, J.F. (2018) The burning coal heap at La Ricamarie, Loire Coal Basin, France, in: Stracher, G.B. Ed. Coal and Peat Fires: A Global Perspective. Volume 5: Case Studies - Advances in Field and Laboratory Research. pp. 301-331.

Triplehorn, D.M., Drake, J., and Layer, P.W. (2000) Preliminary 40Ar/39Ar ages from two units in the Usibelli Group, Healy, Alaska: New light on some old problems. In Pinney, D.S., and Davis, P.K., Eds. Short Notes on Alaska Geology 1999: p. 117–127. Alaska Division of Geological & Geophysical Surveys Professional Report 119I. https://doi.org/10.14509/2691

Wahrhaftig, C., 1987, The Cenozoic section at Suntrana, Alaska.In Hill, M.L., Ed., Cordilleran Section of the Geological Society of America, Centennial Field Guide: Cordilleran Section, Geological Society of America, The Decade of North American Geology (DNAG), Centennial Field Guide 1, p. 445–450, Geological Society of America, Boulder Colorado. https://doi.org/10.1130/0- 8137-5401-1.445.

Wahrhaftig, C., Wolfe, J.A., Leopold, E.B., and Lanphere, M.A.(1969) The Coal-Bearing Group in the Nenana Coal Field, Alaska: Contributions to Stratigraphy. U.S. Geological Survey Bulletin 1274-D, p. D1–D30, https://dggs.alaska.gov/

Wahrhaftig, C. (1951) Geology and coal deposits of the western part of the Nenana coal field, Alaska.In Barnes, F. F. Ed. Coal investigations in south-central Alaska, 1944-46, p. 169-186. U.S. Geological Survey Bulletin 963-E.

Wahrhaftig, C. (1970a) Geologic map of the Healy D-2 quadrangle, Alaska. U.S. Geological Survey Geologic Quadrangle. Map GQ-804. 1 sheet, scale. 1:63,360,

Wahrhaftig, C. (1970b) Geologic map of the Healy D-3 quadrangle, Alaska: U.S. Geological Survey Geologic Quadrangle Map GQ-805. 1 sheet, scale. 1:63,360,

Wahrhaftig, C. (1970c) Geologic map of the Healy D-4 quadrangle, Alaska: U.S. Geological Survey Geologic Quadrangle Map GQ-806. 1 sheet, scale. 1:63,360,

Wahrhaftig, C. (1970d) Geologic map of the Healy ***D-5*** quadrangle, Alaska: U.S. Geological Survey Geologic Quadrangle Map GQ-807. 1 sheet, scale. 1:63,360,

Wahrhaftig, C. (1970e) Geologic map of the Fairbanks A-2 quadrangle, Alaska: U.S. Geological Survey Geologic Quadrangle Map GQ-808. 1 sheet, scale. 1:63,360,

Wahrhaftig, C. (1970f) Geologic map of the Fairbanks A-3 quadrangle, Alaska :US. Geological Survey Geologic Quadrangle Map GQ-809. 1 sheet, scale. 1:63,360,

Wahrhaftig, C. (1970g) Geologic Map of the Fairbanks A-4 Quadrangle, Alaska: U.S. Geological Survey Geologic Quadrangle Map 810, 1 sheet, scale. 1:63,360, https://dggs.alaska.gov/webpubs/usgs/ gq/oversized/gq-0810sht01.pdf

Wahrhaftig, C. (1970h) Geologic map of the Fairbanks A-5 quadrangle, Alaska: U.S. Geological Survey Geologic QuadrangleMap GQ-811.

Wartes, M., Gillis, R.J., Herriott, T.M., Stanley, R.G., Helmold, K.P., Peterson, C.S., and Benowitz, J.A. (2013) Summary of the 2021 Reconnaissance field studies related to petroleum geology of the Nenana Basin, Interior Alaska, Preliminary Interpretive Report 2013-2, 13 p. Division of Geological & Geophysical Surveys, Alaska Geological Survey,

Wolfe, J.A. and Tanai, T. (1980) The Miocene SeldoviaPoint flora from the Kenai Group, Alaska. U.S.Geological Survey Professional Paper 1105, 52 p.

Figure 1. Geologic map of the Nenana Coal Basin, central Alaska Range. Inset map shows the location of the Mystic Creek coal basin portion of the Nenana Coal Basin. Map is based on Wahrhaftig (1970a,b,c,d,e,f,g,h).

Figure 2. Stratigraphy of the central Alaska Range. Modified from Figure 3 of Triplehorn et al. (2000).

Figure 3. Stratigraphy of a portion of the Nenana Coal field area with emphasis on the stratigraphy representative of the Mystic Creek coal basin. The paralava (RR21-1) probably is from the burned coal seam (C & D coal bed). Modified from Figure 3 of Wahrhaftig et al. (1969).

Figure 4. Photograph of hand specimen from the Mystic Creek coal-seam fire. Shown are the sampling locations of XRF samples and thin sections of paralava (RR21-1) and clinker-metasediment (RR21SED1).

Figure 5. Photograph of thin section RR21-1 showing the distribution of the three lithologic domains: sekaninaite-olivine-bearing domain (SP; CS = coarser area), plagioclase-quartz-bearing domains (PQ), and glassy domains (G).

Figure 6. Photomicrographs of selected parts of Paralava (RR21-1) thin section. 6a) sekaninaite-plagioclase domain showing sekaninaite (Sk) microlites exhibiting good (001) cleavage, olivine (Ol), plagioclase, and titanomagnetite. 6b) Photomicrograph of 0.4 mm sekaninaite grain (Sk) exhibiting good (001) cleavage on which red hematite alteration is present. 6c) Photomicrograph of veins extending into a glassy body (G) from the plagioclase-quartz-bearing domain (PQ) bordering it. Titanomagnetite and minor glass are also present. 6d) Photomicrograph showing plagioclase-quartz-bearing vein (PQ) extending into a glassy body (G) from the sekaninaite-plagioclase domain (SP). Note the abrupt loss of sekaninaite (higher birefringent grains) at point vein enters the glassy domain. 6e). Photomicrograph of a cluster of larger plagioclase grains (Pl) in the plagioclase-quartz-bearing domain bordering a glassy body (G). 6f). Photomicrograph of two biaxial positive augite grains (Ag) within the SP domain near the margin of the PQ domain. 6g). Photomicrograph (plane light) of an oval area consisting of an outer zone rich in titanomagnetite (Mg) around a core of sekaninaite (Sk) and euhedral olivine (Ol). 6h). Photomicrograph of a possible sekaninaite microlite (Sk, arrow) in the PQ domain in which its occurrence is minor.

Figure 7. Photograph of a thin section of the metasediment-clinker showing the interfingering of an oxidized red area with the melting black area.

Figure 8. Photomicrograph of the metasediment-clinker (RR21SED1). 8a). Quartz forms the abundant angular grains with low birefringence in the metasediment. The arrow points to a moderately birefringent grain that is possibly sekaninaite. The thin elongate grains are too small to identify. 8b). Photomicrograph of flow structure in black clinker produced by aligned flattened vesicles and prismatic grains. 8c). Photomicrograph (plain light) of lobe of black clinker within

red oxidized portion. 8d.) Photomicrograph (plain light) showing a vein of PQ domain in black clinker.

Figure 9. Photomicrographs showing locations of grains analyzed by micropobe. 9a). Sekaninaite-Plagioclase (SP) domain; 9b). Glass domain; 9c). Plagioclase-Quartz (PQ) domain. SK- Sekaninaite; Ol-Olivine; FS-Feldspar; Tm-Titanomagnetite; G-Glass; MC-minor crystallites; Si-Silica. MM-Unidentified Ti-AL-Fe opaque mineral. Numbers following mineral identification refer to On-Line Data Table 1.

Figure 10. XRD mineral analyses of paralava and host sediment. 11a). Paralava; 11b). Metasediment-clinker.

Figure 11. XRF analyses of paralava and metasediment-clinker plotted on the alkali-silica diagram of LeBas et al (1986). G1 and G2 are identified in Figure 10 and Table 2. The number's locations are identified in On-Line Table 1.

Figure 12. Mystic coal subbasin paralava and metasediment-clinker compositions and crystallization paths plotted in the system FeO–Al2O3–SiO2 of Schairer and Yagi (1952) and with Fe-cordierite renamed as sekaninaite. Arrows indicate direction of falling temperature, and relevant invariant and reaction points are listed. Modified from Grapes et al. (2011).

Figure 13. Paralava and host sediment rare earth data plotted on the on bulk Earth diagrams of Rudnick and Fountain (1995) 14a) and Hickley et al. (1986) 14b). showing the complete melting of the host sediment to form the paralava.

Table 1. Modal analyses of the paralava*

Phase	Sekaninaite	Plagioclase	Quartz	Olivine	Opaques	Glass	total
SP domains*	13.4	56.7	-	12.3	17.6	-	100.0
PQ domains*	trace	59.4	9.7	-	30.9	5.5	100.0
Glassy domains	trace	15.1	10.3	-	2.0	72.6	100.0

*SP = Sekaninaite and plagioclase rich domains; PQ = plagioclase and quartz rich domains; Due to small size of areas, modal analyses based on counts of 700 points, 217 points, and 252 points for the SP domains, PQ domains, and glassy domains respectively.

Table 2. XRF analyses for the Paralava and Clinker-metasediment

	Sample		**RR1SED-1**		**RR21-1**
	Clinker-metasediment			Paralava	
Major elements (wt %		**SiO2**	59.67	**SiO2**	58.44

oxides)				
	TiO2	0.956	**TiO2**	0.923
	Al2O3	23.94	**Al2O3**	23.00
	FeO*	7.62	**FeO***	10.31
	MnO	0.122	**MnO**	0.154
	MgO	1.45	**MgO**	1.55
	CaO	0.51	**CaO**	1.15
	Na2O	0.30	**Na2O**	0.26
	K2O	3.46	**K2O**	2.86
	P2O5	0.112	**P2O5**	0.541
	LOI (%)	0.88	**LOI (%)**	0.00
	sumMaj+LOI	99.00	**sumMaj+LOI**	99.16
	sumAll	99.25	**sumAll**	99.52
Volatiles (wt %)	**F >=**	0.00	**F >=**	0.08
	Cl >=	0.00	**Cl >=**	0.00
	SO3 >=	0.00	**SO3 >=**	0.00
Volatiles (ppm)	**Br >=**	1	**Br >=**	0
	As >=	6	**As >=**	9
Trace elements (ppm)	**Ni**	41	**Ni**	52
	Cr	108	**Cr**	109
	V	134	**V**	144
	Sc	20	**Sc**	20
	Cu	38	**Cu**	20
	Zn	156	**Zn**	374
	Ga	31	**Ga**	32
	Ba	1041	**Ba**	1066
	Rb	170	**Rb**	153
	Cs	6	**Cs**	6
	Sr	64	**Sr**	70
	Y	44	**Y**	47
	Zr	273	**Zr**	261
	Hf	9.0	**Hf**	8.2
	Nb	24.8	**Nb**	24
	Ta	1	**Ta**	1
	Mo	0	**Mo**	2
	La	62	**La**	65
	Ce	118	**Ce**	122
	Nd	50	**Nd**	53
	Sm	10.5	**Sm**	10.8
	Dy	5.6	**Dy**	7.2
	Yb	3.2	**Yb**	4.6
	Th	32	**Th**	30
	U	6	**U**	6
	Tl	2	**Tl**	1
	Pb	24	**Pb**	93
	Sn	4	**Sn**	12
	Bi	0	**Bi**	0
	Sb	1	**Sb**	2

Analyses by Hamiltion Labs

Table 3a. Mixing Run 1	The Hybrid magma is RR21-1 Paralava	
Coef	Solid	Magma
0.040	0.4%	Al-Ti-Fe Oxide
0.031	3.1%	Plagioclase Feldspar
0.502	50.2%	Glass
0.426	42.6%)	Sekaninate

	SiO_2	TiO_2	Al_2O_3	FeO	MnO	MgO	CaO	Na_2O	K_2O	P_2O_5
Obs	58.92	0.93	23.19	10.39	0.16	1.56	1.16	0.26	2.88	0.55
Calc	59.01	0.71	23.24	10.46	0.10	1.84	1.27	0.07	3.21	0.05
Diff*Wt	-0.04	0.23	-0.03	-0.07	0.06	-0.27	-0.1	0.20	-0.33	0.49
1 Sigma	2.504	0.209	2.81	1.587	0.081	0.041	0.674	0.054	0.841	0.704
Sum of squares of residuals= 0.539										

Table 3b. Mixing Run 2	The Hybrid magma is RR21-1 Paralava	
Coef	Solid	Magma
0.058	5.8%	Al-Ti-Fe Oxide
0.028	2.8%	Plagioclase Feldspar
-0.020	-2.0%	Fayalite Olivine
0.513	51.3%	Glass
0.421	42.1%	Sekaninaite

	SiO_2	TiO_2	Al_2O_3	FeO	MnO	MgO	CaO	Na_2O	K_2O	P_2O_5
Obs	58.92	0.93	23.19	10.39	0.16	1.56	1.16	0.26	2.88	0.55
Calc	58.87	0.86	23.35	10.43	0.08	1.75	1.22	0.07	3.28	0.05
Diff*Wt	0.02	0.07	-0.08	-0.03	0.08	-0.18	-0.06	0.20	-0.39	0.49
1 Sigma	2.504	0.209	2.81	1.587	0.081	0.041	0.674	0.054	0.841	0.704
Sum of squares of residuals= 0.492										

Table 3c. Mixing Run 3	The Hybrid magma is RR21-1 Paralava	
Coef	Solid	Magma
0.005	0.5%	Ilmenite
0.036	3.6%	Al-Ti-Fe Oxide
0.029	2.9%	Plagioclase Feldspar
0.499	49.9%	Glass
0.430	43.0%	Sekaninaite

	SiO_2	TiO_2	Al_2O_3	FeO	MnO	MgO	CaO	Na_2O	K_2O	P_2O_5
Obs	58.92	0.93	23.19	10.39	0.16	1.56	1.16	0.26	2.88	0.55
Calc	58.89	0.94	23.23	10.41	0.10	1.85	1.24	0.07	3.20	0.05
Diff*Wt	0.01	-0.01	-0.02	-0.02	0.06	-0.29	-0.08	-0.31	0.50	0.05
1 Sigma	2.504	0.209	2.81	1.587	0.081	0.041	0.674	0.054	0.841	0.704
Sum of squares of residuals= 0.478										

Table 4. Fractional Crystallization	The Parent magma is RR21-1 Paralava	
Coef	Solid	Magma
0.012	2.2%	Ilmenite
0.016	2.9%	Fayalite Olivine
0.048	9.1%	Plagioclase Feldspar
0.456	85.8%	Sekaninate
0.470		Daughter (Glass)

	SiO_2	TiO_2	Al_2O_3	FeO	MnO	MgO	CaO	Na_2O	K_2O	P_2O_5
Obs	58.92	0.93	23.19	10.39	0.16	1.56	1.16	0.26	2.88	0.55
Calc	58.66	0.74	23.10	10.26	0.16	1.95	1.12	0.01	3.70	0.45
Diff*Wt	0.26	0.18	0.09	0.13	0	-0.39	0.04	0.26	-0.81	0.10
1 Sigma	2.504	0.209	2.81	1.587	0.081	0.041	0.674	0.054	0.841	0.704
Sum of squares of residuals= 1.014										

Figure 1

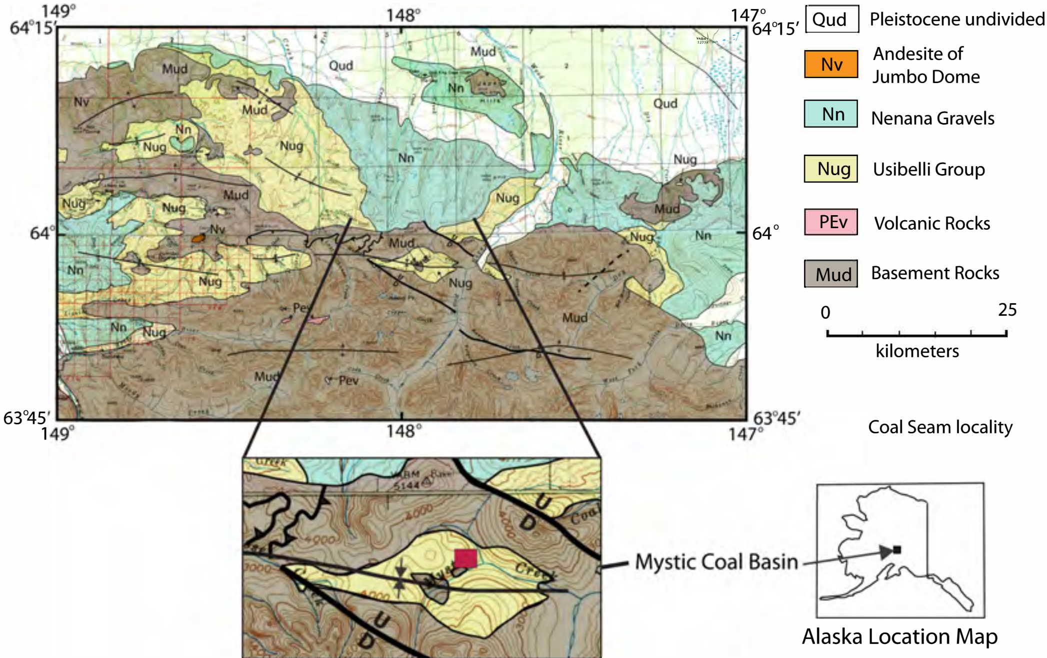

149°
148°
147°
64°15′
64°15′
64°
64°
63°45′
63°45′
149°
148°
147°
Qud
Mud
Nv
Nn
Nug
Pev
Qud
Pleistocene undivided
Nv
Andesite of Jumbo Dome
Nn
Nenana Gravels
Nug
Usibelli Group
PEv
Volcanic Rocks
Mud
Basement Rocks
0
25
kilometers
Coal Seam locality
Mystic Coal Basin
Alaska Location Map

Figure 2

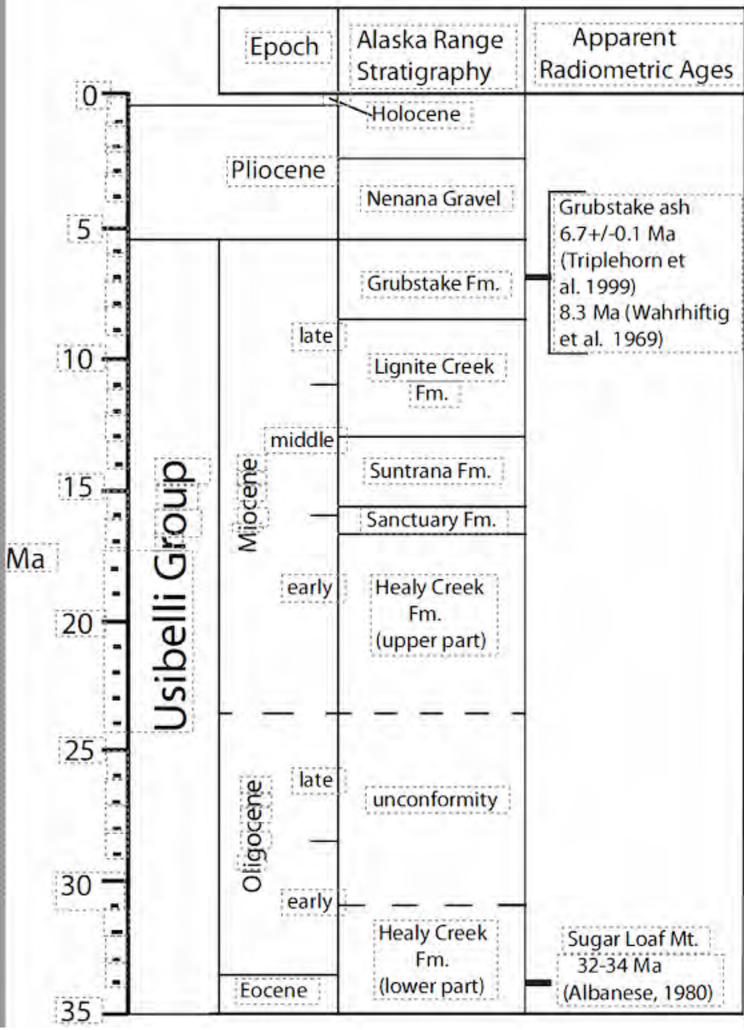

Epoch
Alaska Range Stratigraphy
Apparent Radiometric Ages
Ma
0
5
10
15
20
25
30
35
Usibelli Group
Holocene
Pliocene
Miocene
late
middle
early
Oligocene
late
early
Eocene
Nenana Gravel
Grubstake Fm.
Lignite Creek Fm.
Suntrana Fm.
Sanctuary Fm.
Healy Creek Fm. (upper part)
unconformity
Healy Creek Fm. (lower part)
Grubstake ash 6.7+/-0.1 Ma (Triplehorn et al. 1999) 8.3 Ma (Wahrhiftig et al. 1969)
Sugar Loaf Mt. 32-34 Ma (Albanese, 1980)

Figure 3

Coal Bed No. 2
Coal Bed No. 1
G Coal Bed
F Coal Bed
E Coal Bed
Burned Coal
C &D Coal Bed
B Coal Bed
A Coal Bed
Suntrana Formation
Type Section of the Sanctuary Formation
Type Section of the Healy Creek Formation
Birch Creek Schist
Meters
60
30
0

Figure 4

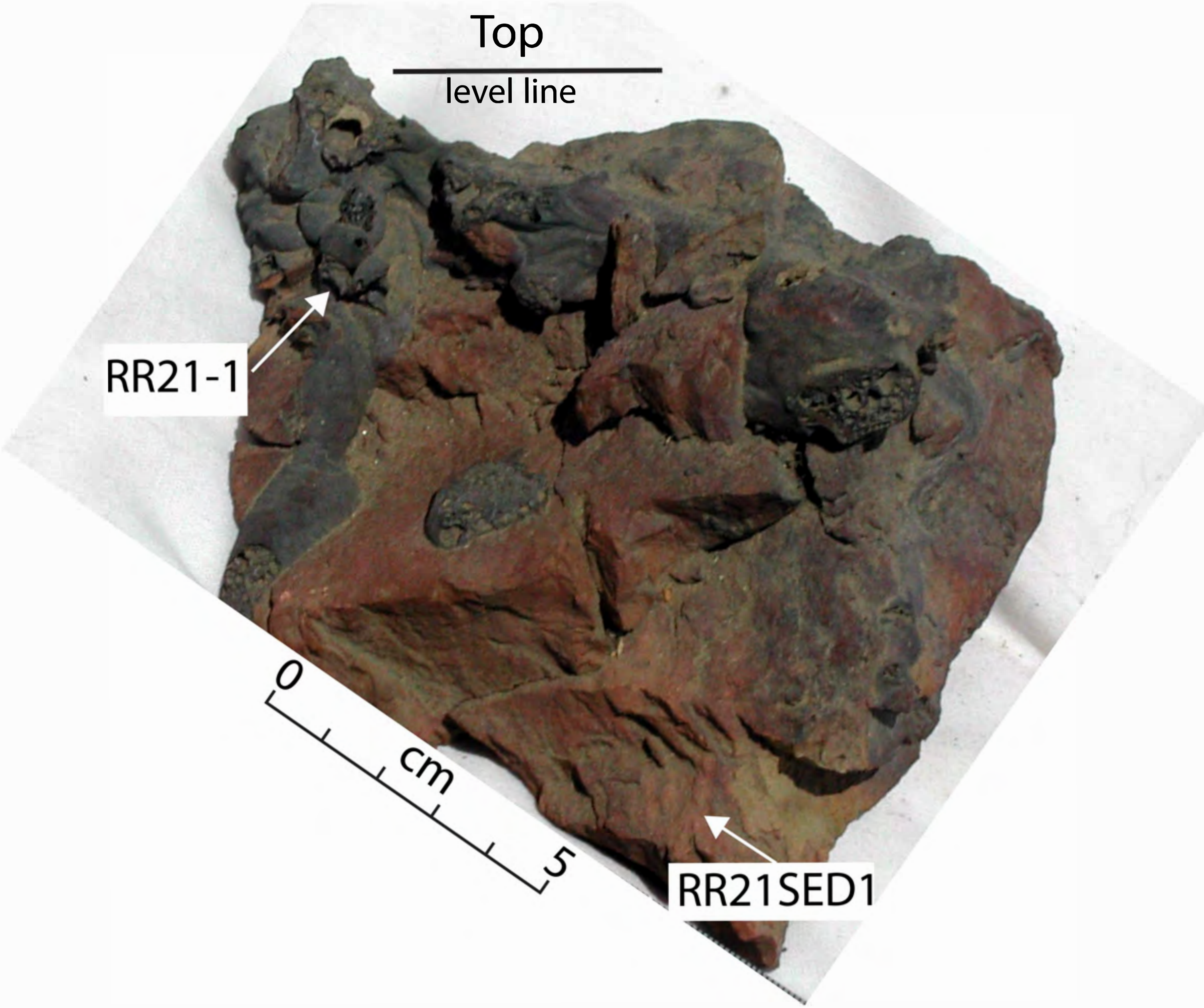

Figure 5

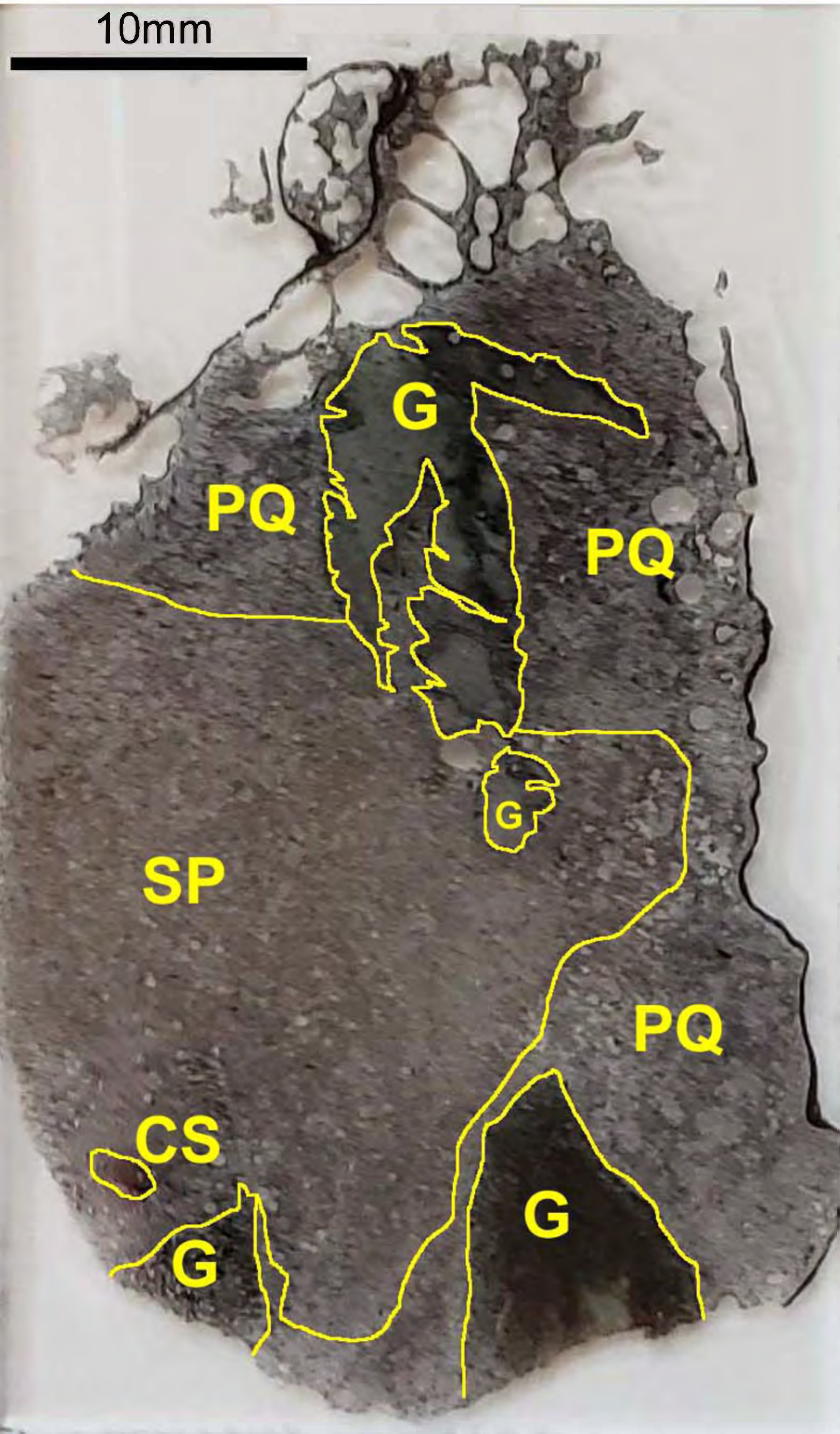

Figure 6 (a-d)

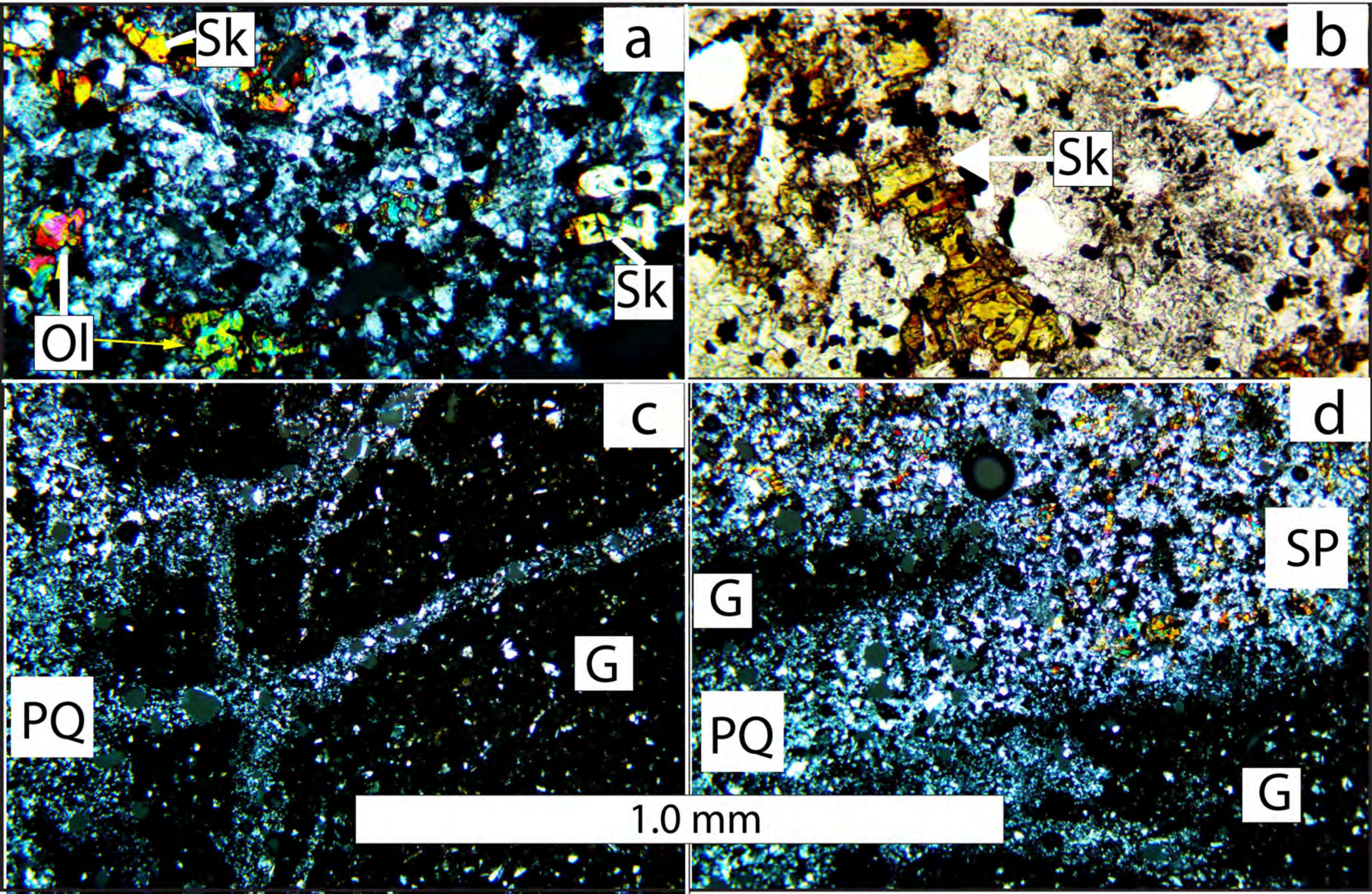

Figure 6 (e-h)

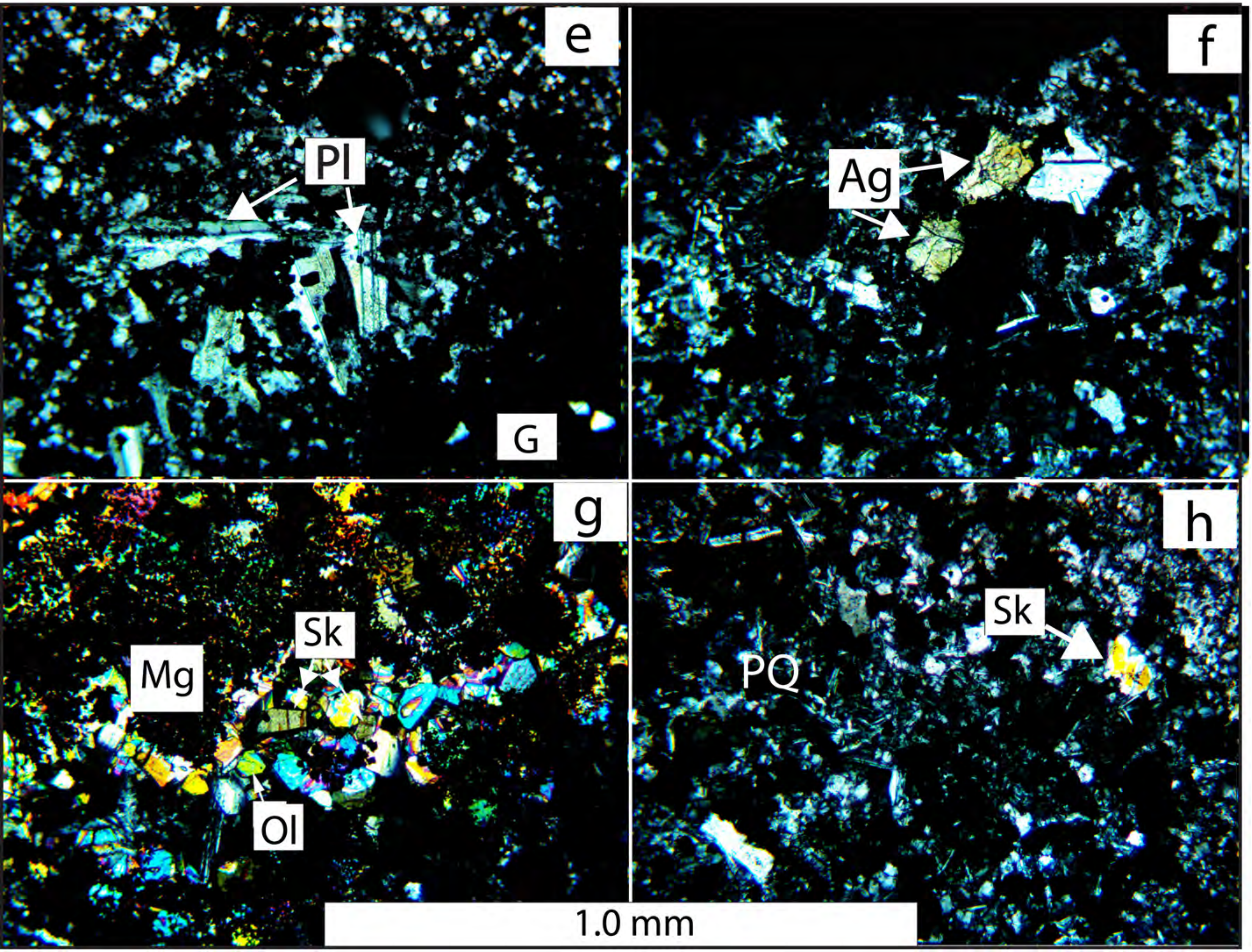

Figure 7

Figure 8

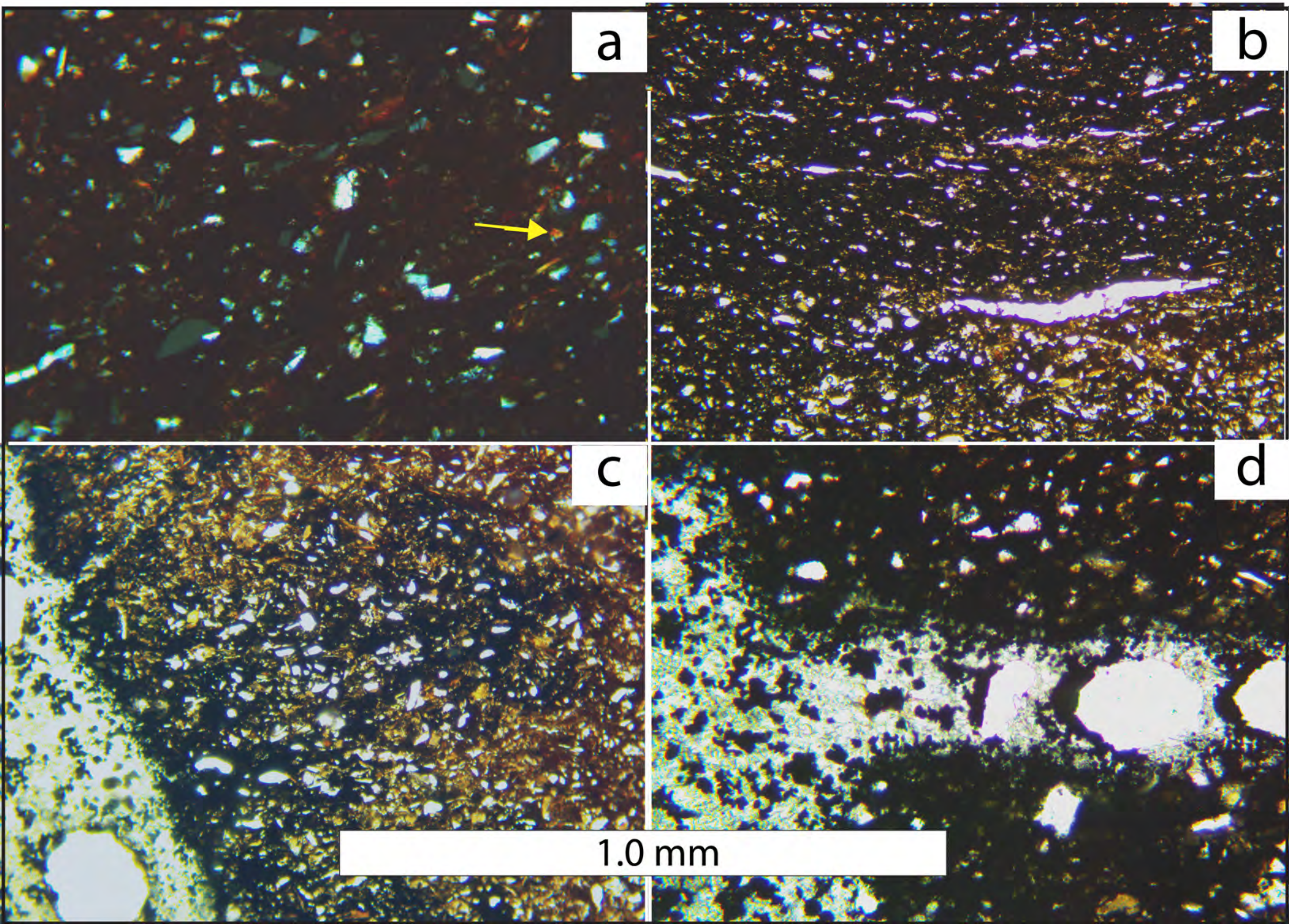

Figure 9

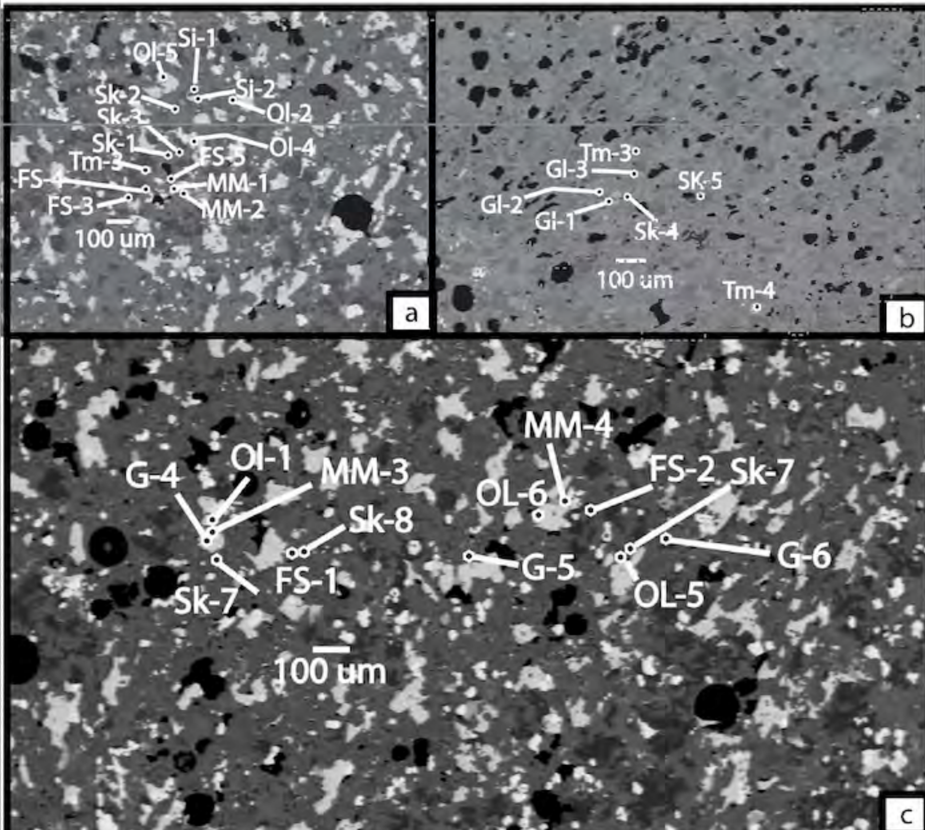

Ol-5
Si-1
Sk-2
Si-2
Ol-2
Sk-3
Sk-1
Ol-4
Tm-3
FS-5
FS-4
MM-1
FS-3
MM-2
100 um
a
Tm-3
Gl-3
SK-5
Gl-2
Gl-1
Sk-4
100 um
Tm-4
b
MM-4
G-4
Ol-1
MM-3
FS-2
Sk-7
OL-6
Sk-8
G-6
G-5
FS-1
OL-5
Sk-7
100 um
c

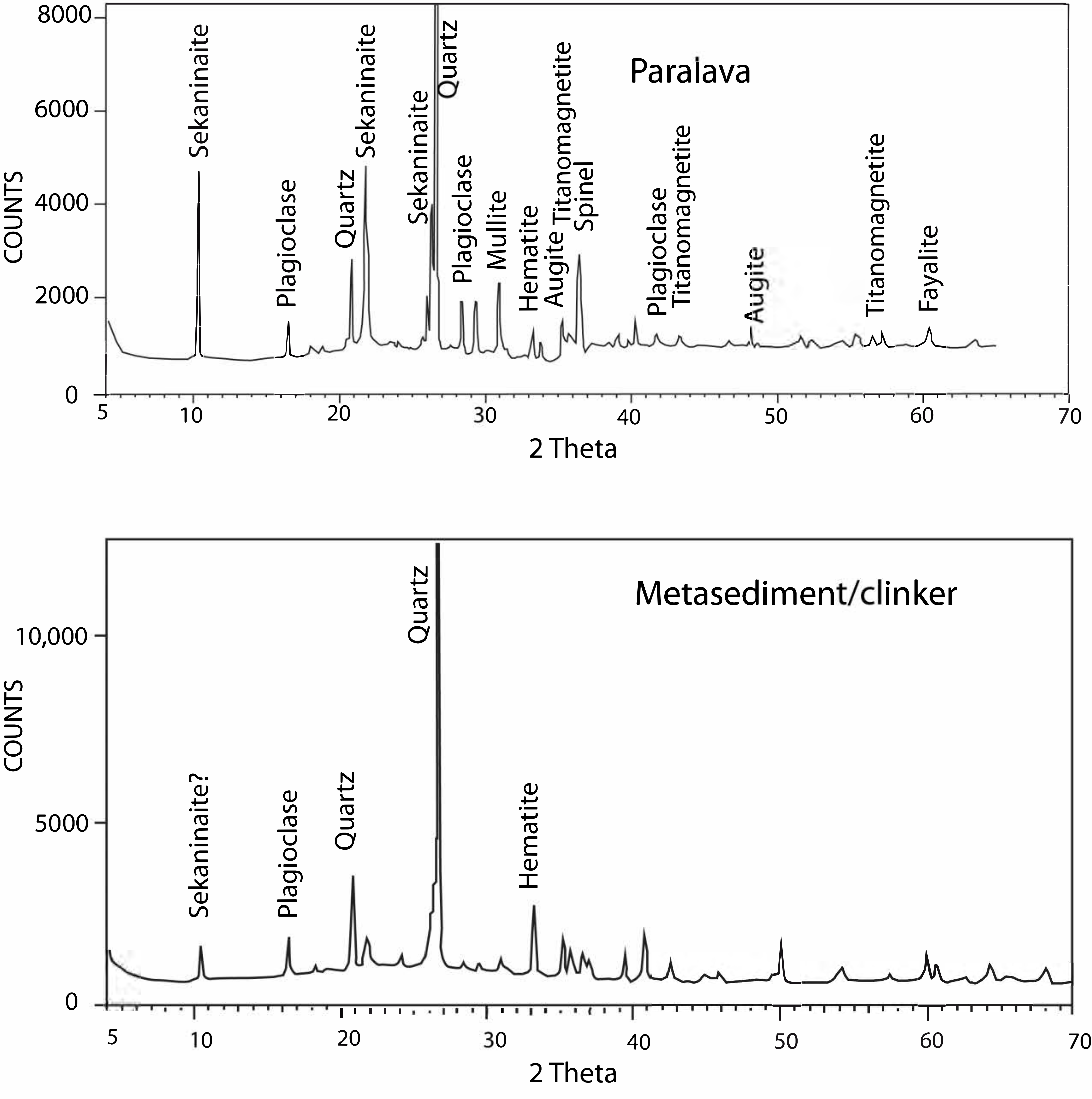
Paralava
COUNTS
2 Theta
Sekaninaite
Plagioclase
Quartz
Sekaninaite
Sekaninaite
Quartz
Plagioclase
Mullite
Hematite
Augite
Titanomagnetite
Spinel
Plagioclase
Titanomagnetite
Augite
Titanomagnetite
Fayalite
Metasediment/clinker
Sekaninaite?
Plagioclase
Quartz
Quartz
Hematite
10,000
5000
8000
6000
4000
2000
0
5
10
20
30
40
50
60
70

Figure 10

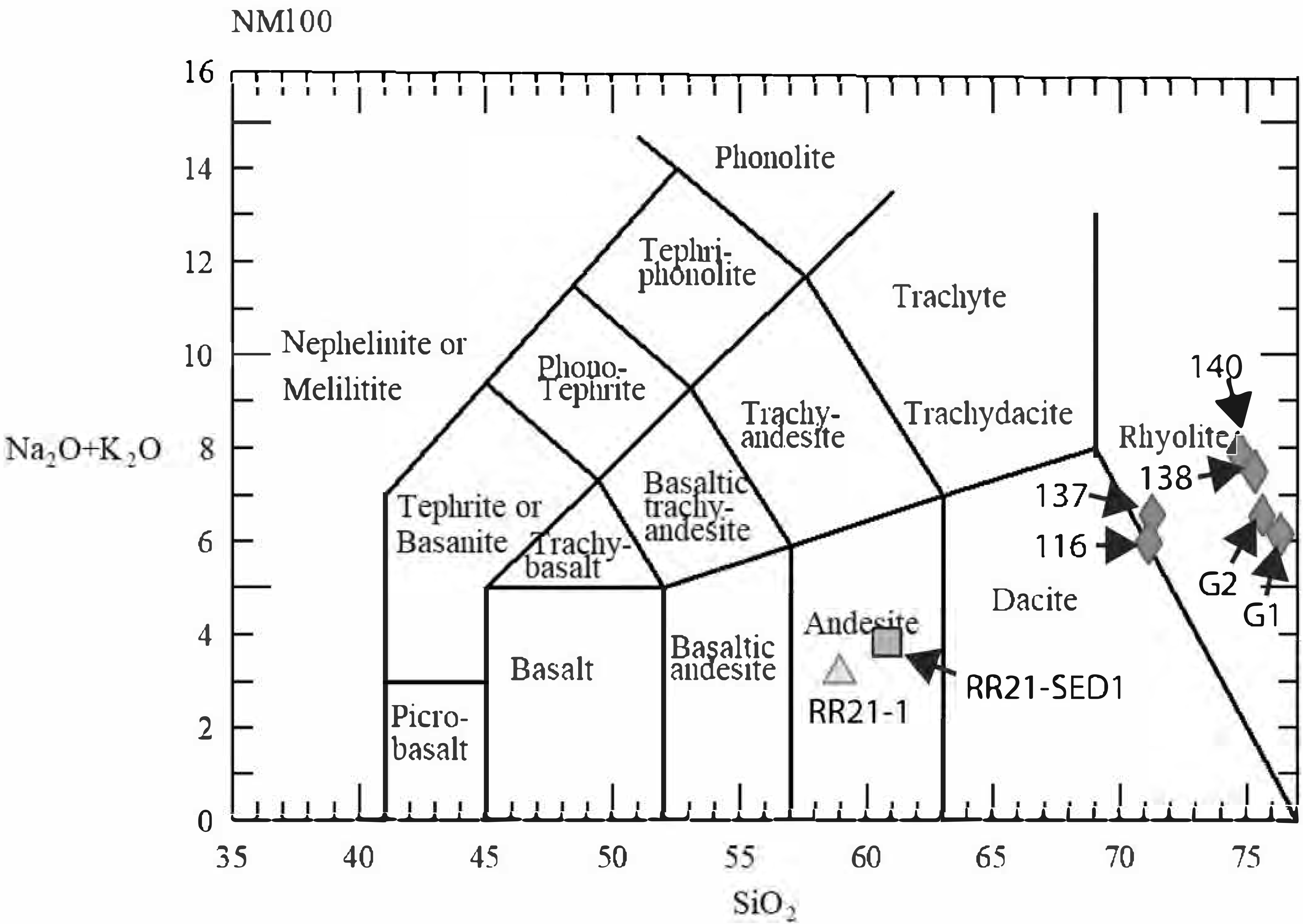
NM100
16
14
12
10
8
6
4
2
0
35
40
45
50
55
60
65
70
75
Na2O+K2O
SiO2
Phonolite
Tephri-
phonolite
Trachyte
Nephelinite or
Melilitite
Phono-
Tephrite
Trachy-
andesite
Trachydacite
Rhyolite
Basaltic
trachy-
andesite
Tephrite or
Basanite
Trachy-
basalt
Dacite
Andesite
Basaltic
andesite
Basalt
Picro-
basalt
140
138
137
116
G2
G1
RR21-SED1
RR21-1

Figure 11

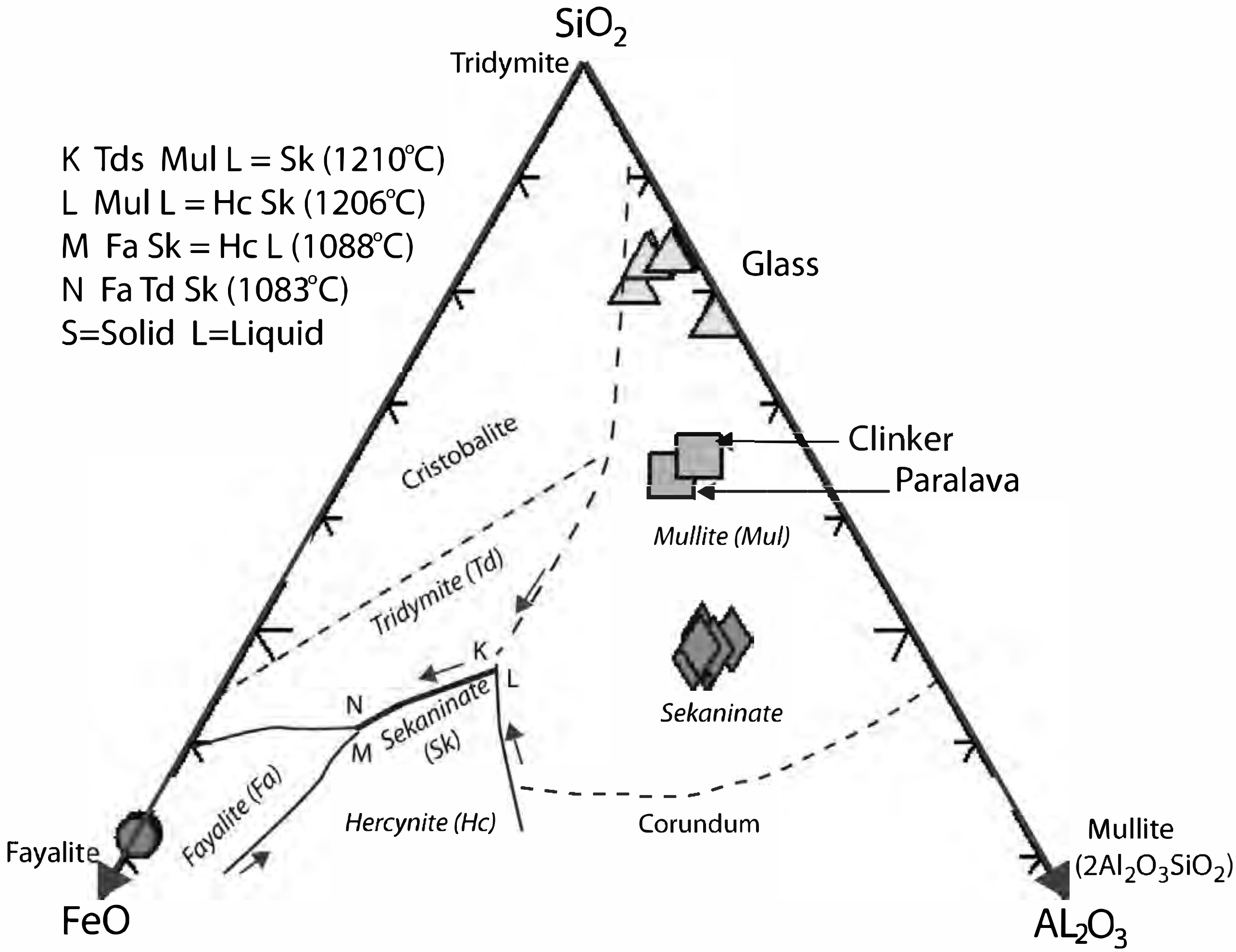

SiO_2
Tridymite
K Tds Mul L = Sk (1210°C)
L Mul L = Hc Sk (1206°C)
M Fa Sk = Hc L (1088°C)
N Fa Td Sk (1083°C)
S=Solid L=Liquid
Glass
Clinker
Paralava
Cristobalite
Mullite (Mul)
Tridymite (Td)
K
L
N
M
Sekaninate (Sk)
Sekaninate
Fayalite (Fa)
Hercynite (Hc)
Corundum
Fayalite
Mullite
$(2Al_2O_3SiO_2)$
FeO
AL_2O_3

Figure 12

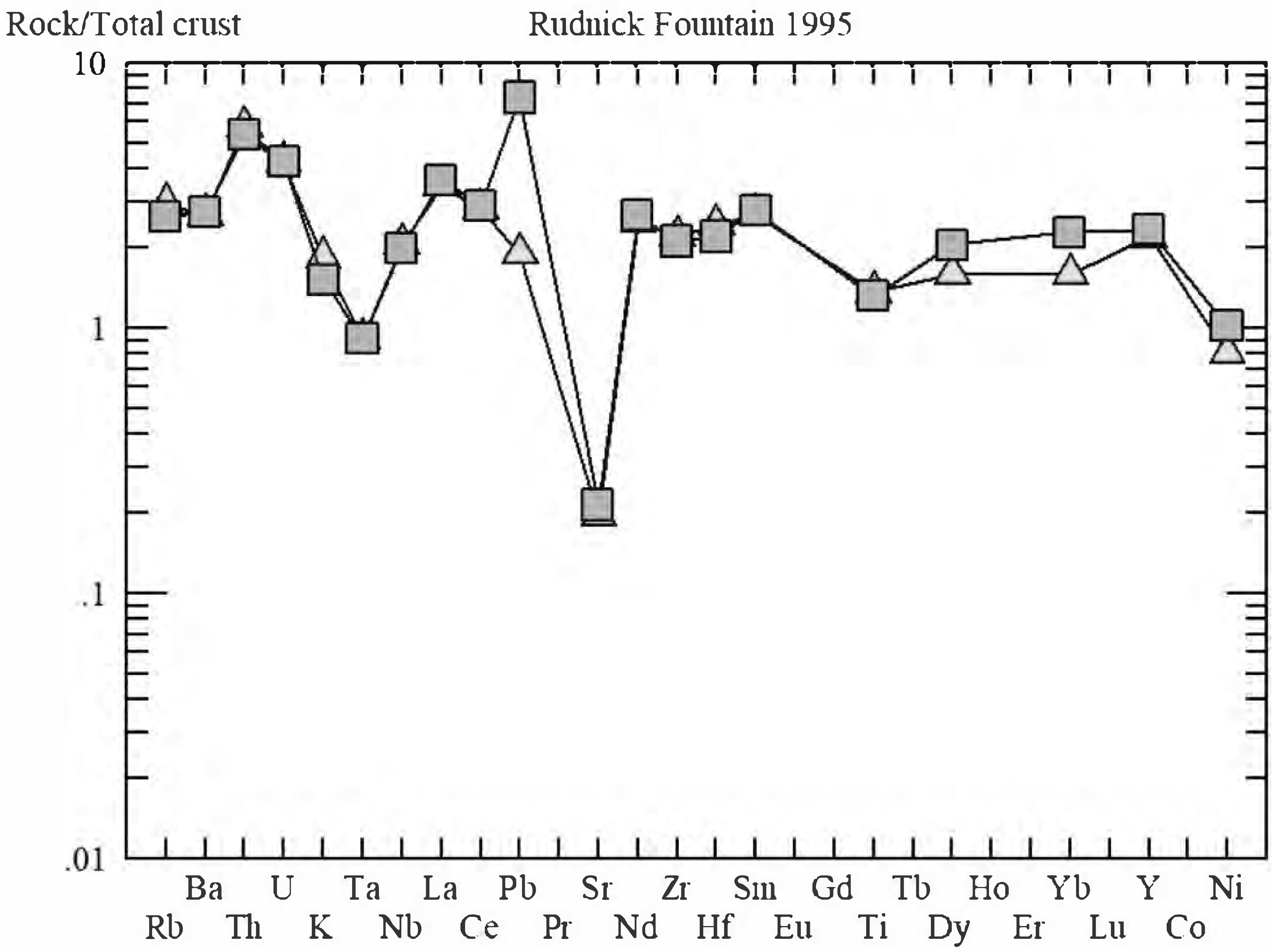
Rock/Total crust
Rudnick Fountain 1995
10
1
.1
.01
Ba U Ta La Pb Sr Zr Sm Gd Tb Ho Yb Y Ni
Rb Th K Nb Ce Pr Nd Hf Eu Ti Dy Er Lu Co

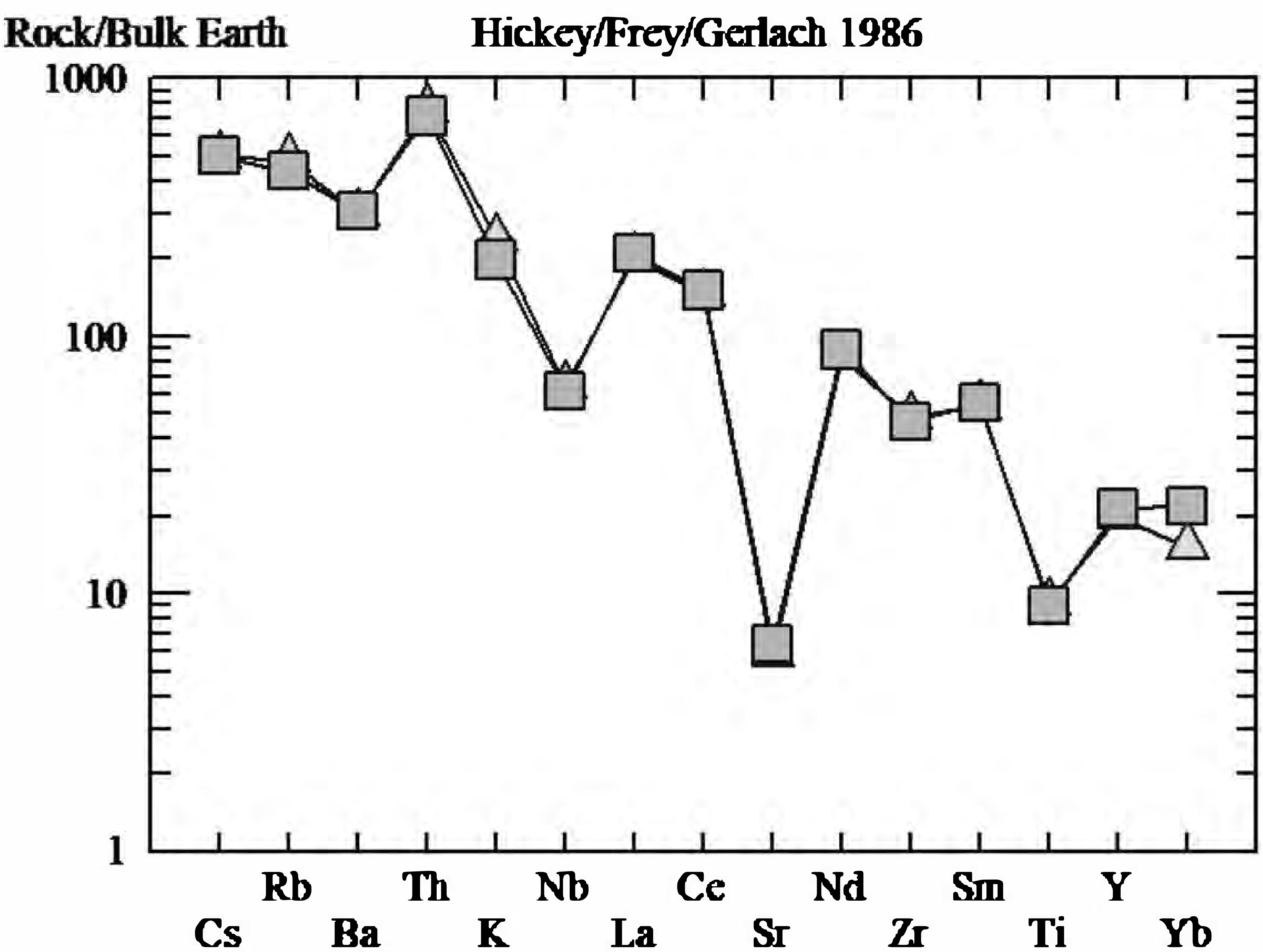
Rock/Bulk Earth
Hickey/Frey/Gerlach 1986
1000
100
10
1
Rb Th Nb Ce Nd Sm Y
Cs Ba K La Sr Zr Ti Yb

Figure 13